

UC San Diego

UC San Diego Previously Published Works

Title

A Drosophila Model for Clostridium difficile Toxin CDT Reveals Interactions with Multiple Effector Pathways

Permalink

<https://escholarship.org/uc/item/1135g3g8>

Journal

iScience, 23(2)

ISSN

2589-0042

Authors

Schwartz, Ruth
Guichard, Annabel
Franc, Nathalie C
[et al.](#)

Publication Date

2020-02-01

DOI

10.1016/j.isci.2020.100865

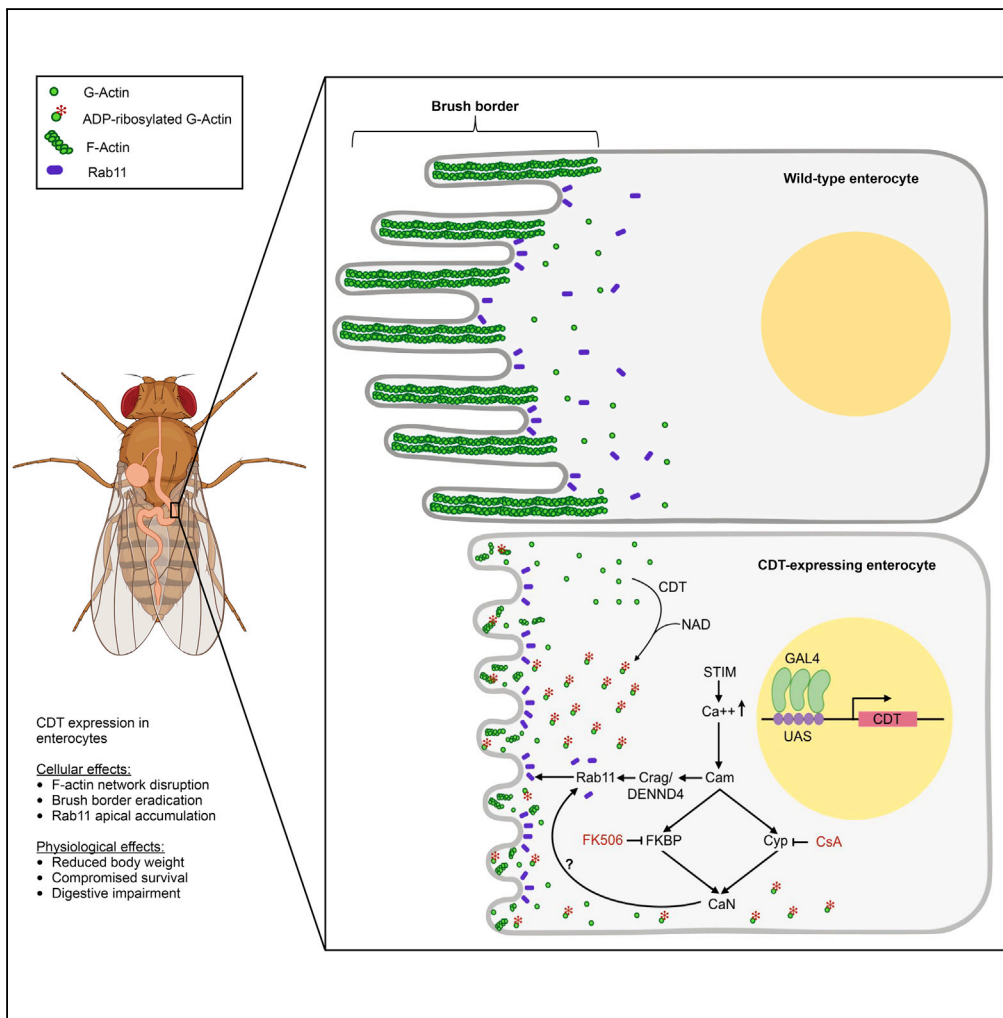
Copyright Information

This work is made available under the terms of a Creative Commons Attribution-NonCommercial-NoDerivatives License, available at <https://creativecommons.org/licenses/by-nc-nd/4.0/>

Peer reviewed

Article

A *Drosophila* Model for *Clostridium difficile* Toxin CDT Reveals Interactions with Multiple Effector Pathways



Ruth Schwartz,
Annabel
Guichard,
Nathalie C. Franc,
Sitara Roy, Ethan
Bier

ebier@ucsd.edu

HIGHLIGHTS

We created transgenic flies expressing the *Clostridium difficile* CDTa toxin

CDTa impairs digestive functions, F-actin networks, and Rab11 distribution

Rab11 is a key mediator of CDTa-induced phenotypes

The Ca⁺⁺/Calmodulin pathway is required for the cellular response to CDTa

Schwartz et al., iScience 23, 100865
February 21, 2020 © 2020 The Author(s).
<https://doi.org/10.1016/j.isci.2020.100865>



Article

A *Drosophila* Model for *Clostridium difficile* Toxin CDT Reveals Interactions with Multiple Effector Pathways

Ruth Schwartz,¹ Annabel Guichard,^{1,2} Nathalie C. Franc,^{3,4} Sitara Roy,¹ and Ethan Bier^{1,2,5,*}

SUMMARY

Clostridium difficile infections (CDIs) cause severe and occasionally life-threatening diarrhea. Hyper-virulent strains produce CDT, a toxin that ADP-ribosylates actin monomers and inhibits actin polymerization. We created transgenic *Drosophila* lines expressing the catalytic subunit CDTa to investigate its interaction with host signaling pathways *in vivo*. When expressed in the midgut, CDTa reduces body weight and fecal output and compromises survival, suggesting severe impairment of digestive functions. At the cellular level, CDTa induces F-actin network collapse, elimination of the intestinal brush border, and disruption of intercellular junctions. We confirm toxin-dependent re-distribution of Rab11 to enterocytes' apical surface and observe suppression of CDTa phenotypes by a Dominant-Negative form of Rab11 or RNAi of the dedicated Rab11GEF Crag (DENND4). We also report that Calmodulin (Cam) is required to mediate CDTa activity. In parallel, chemical inhibition of the Cam/Calcineurin pathway by Cyclosporin A or FK506 also reduces CDTa phenotypes, potentially opening new avenues for treating CDIs.

INTRODUCTION

Clostridium difficile (*C. difficile*) is a gram-positive anaerobic sporogenic bacterium that causes gastrointestinal infections mostly in elderly or frail individuals and in patients treated with antibiotics (Bartlett, 2002, 2006; Ciaran, 2008). Subsequent alterations in the intestinal microbiome provide favorable conditions for *C. difficile* growth and infection, which cause about 20% of all antibiotic-associated diarrhea cases (Abt et al., 2016; Schwan et al., 2009). Outbreaks of *C. difficile* infection (CDI) have increased progressively in Western countries, and fatalities sum to 29,000 deaths per year in the United States alone (Lessa et al., 2015). Extensive reviews of CDIs point to their growing impact on public health and the need for alternative therapies (Aktories et al., 2017; Gerding et al., 2014).

CDI pathogenesis has been mostly attributed to two related toxins secreted by *C. difficile*: toxin A (TcdA) and toxin B (TcdB) (Bartlett, 2002; Just and Gerhard, 2004; Kelly and LaMont, 2008; Voth and Ballard, 2005). Both toxins glucosylate and irreversibly inactivate small GTPases of the Rho/Rac/Cdc42 family, leading to disruptions in F-actin networks, subsequent epithelial damage, and increased barrier permeability due to loss of tight junction integrity (Aktories et al., 2018; Just et al., 1995a, 1995b; Papatheodorou et al., 2018). In addition, 35% of *C. difficile* isolates express a third toxin, *C. difficile* transferase (CDT), known to confer hyper-virulence during infection (Geric et al., 2004; Goncalves et al., 2004; Stubbs et al., 2000), and belonging to a conserved family of binary effectors from various enteric pathogens such as *C. botulinum* (C2 toxin), *C. perfringens* (BEC), and *B. cereus* (VIP) (Stiles et al., 2014). The binary CDT toxin consists of an enzymatic unit, CDTa, which covalently modifies actin monomers, and a transport unit, CDTb, which binds CDTa and allows its entry into target cells via the lipolysis-stimulated lipoprotein receptor (LSR) (Barth et al., 2004; Papatheodorou et al., 2011; Popoff et al., 1988). Once in the cytosol, CDTa blocks actin polymerization via ADP-ribosylation of G-actin at Arginine 177 (Aktories et al., 1986; Vandekerckhove et al., 1987). As a consequence, F-actin elongation is inhibited, resulting in further depolymerization of actin filaments (Aktories and Wegner, 1992; Wegner and Aktories, 1988). Recent studies in cultured human enterocytes (CACO-2) have shown that CDT induces the formation of long microtubule-based protrusions, which promote bacterial adherence to host cells (Schwan et al., 2009). This process, mediated by calcium (Ca²⁺) signaling and the Ca²⁺-sensor Stim1, involves the rerouting of vesicles loaded with fibronectin to the apical plasma membrane (Schwan et al., 2014). The small GTPase Rab11 involved in endocytic recycling may play a role in this process, as these Fibronectin-rich vesicles also co-localize with Rab11. Thus, despite its deceptively simple mode of action, CDT acts in a threshold-dependent fashion to deregulate particular

¹Section of Cell and Developmental Biology, University of California, San Diego, La Jolla, CA 92093-0335, USA

²Tata Institute for Genetics and Society-UCSD, La Jolla, CA 92093-0335, USA

³Franc Consulting, San Diego, CA 92117-3314, USA

⁴The Scripps Research Institute, La Jolla, CA 92037, USA

⁵Lead Contact

*Correspondence: ebier@ucsd.edu

<https://doi.org/10.1016/j.isci.2020.100865>



signaling pathways thereby eliciting specific cellular responses that exacerbate its general effect of disrupting F-actin networks (Aktories et al., 2018). To parse these complex interactions in the context of a live organism, we made use of the powerful genetic model *Drosophila melanogaster*, a widely successful tool for dissecting pathogenic mechanisms and strategies underlying host defense (Bier and Guichard, 2012; Buchon et al., 2013; Capo et al., 2019). For example, previous studies employed transgenic flies to express bacterial effectors such as *Pseudomonas* ExoS (Avet-Rochex et al., 2007), *Helicobacter* VacA (Botham et al., 2008), anthrax toxins (EF and LF) (Guichard et al., 2010; Guichard et al., 2017), or Cholera toxin (Ctx) (Blow et al., 2005) (Guichard et al., 2013) to uncover novel aspects of the host cellular response.

In this report, we establish a *Drosophila* system for the *in vivo* study of CDTa. We show that expression of CDTa in the gut reduces pupal and adult body size and weight, as well as viability and longevity. We observe that CDTa severely disrupts the F-actin network in several tissues with a consequent loss of epithelial junction integrity. We further demonstrate that the defects caused by CDTa expression can be partially rescued through inhibition of Rab11. Consistent with the known involvement of Ca^{2+} signaling in the cellular response to CDT, two Ca^{2+} sensors, Stim and Calmodulin (Cam), block the effects of CDTa during fly development. In parallel, Cyclosporin A and FK506, compounds that inhibit Calmodulin signaling via direct interaction with Cyclophilin and FKBP12, respectively, suppress CDTa wing phenotypes. In aggregate, findings in this study delineate a functional connection between CDTa and Calmodulin, opening the way to therapeutic approaches based on chemical modulation of the Calmodulin/Calcineurin pathway for treatment of infection by hypervirulent *C. difficile*.

RESULTS

CDTa Expression Reduces Body Size, Weight, Survival, and Longevity

Drosophila melanogaster has been employed successfully as a genetic model system to decipher functional aspects of various bacterial toxins in the context of a whole organism (Botham et al., 2008; Avet-Rochex et al., 2007; Bier and Guichard, 2012; Buchon et al., 2013; Capo et al., 2019; Luo et al., 2019). In this study we focus our analysis on the CDT toxin, which is secreted by hypervirulent strains of *C. difficile*. Paralleling strategies employed in previous studies, we created UAS-CDTa transgenic lines in which expression of the catalytic subunit CDTa can be induced in the presence of the GAL4 trans-activator (Brand and Perrimon, 1993). CDTa was expressed in various tissues by crossing flies from these lines to individuals expressing GAL4 with various temporal and tissue specificities. When expressed in the relevant midgut (using NP1-GAL4) or hindgut (using hindgut-GAL4) tissues during development, CDTa led to a significant reduction in body size at pupal and adult stages (Figures 1A and 1B). This phenotype was accompanied by a 25% and 35% reduction in body weight in male and female adult flies, respectively (Figure 1C). Approximately 20% of emerging adults carried the UAS-CDTa transgene (Figure 1D), deviating substantially from the expected 50% rate of Mendelian inheritance, indicating a severe fitness cost during pre-adult stages.

We assessed whether CDTa expression compromises lifespan by conducting a comparative survival assay. In this experiment, CDTa expression was temporally delayed until adulthood using the temperature-sensitive tubGAL80ts inhibitor, which blocks GAL4 function at temperatures below 25°C (McGuire et al., 2004). Control flies (NP1GAL4 tubGAL80ts/+) and flies conditionally expressing CDTa (NP1GAL4 tubGAL80ts > CDTa) were raised at room temperature (RT) and transferred to 29°C a week after hatching to induce adult CDTa expression. Survival over time was monitored daily, revealing a significant CDTa-dependent reduction in fly longevity (Figure 1E). Flies expressing CDTa survived only to 5–17 days, whereas all control flies not expressing the toxin lived well beyond the final time point sampled of 23 days (Figure 1E).

In summary, CDTa expression drastically reduces fly body size and weight, compromising early viability and adult longevity. This cluster of phenotypes suggests that CDTa impairs essential functions in intestinal cells.

CDTa Expression Diminishes Fecal Output and Causes Crop Enlargement

C. difficile infection (CDI) in human patients causes severe gastrointestinal infections, inflammatory diarrhea, intestinal blockage, and perforation (Bartlett, 2002, 2006; Ciaran, 2008). We investigated the final outcome of CDTa expression in the fly adult digestive system by measuring the effect of CDTa on fecal matter production. Flies were grown at RT and, a week after hatching, transferred to 31°C to induce CDTa expression. Animals were fed a sucrose solution supplemented with green dye to help visualize the gut, and fecal output was collected on transparent film, which was then scanned and quantified using the ImageJ software (Schindelin et al., 2012). When compared with control flies, which produced ample fecal

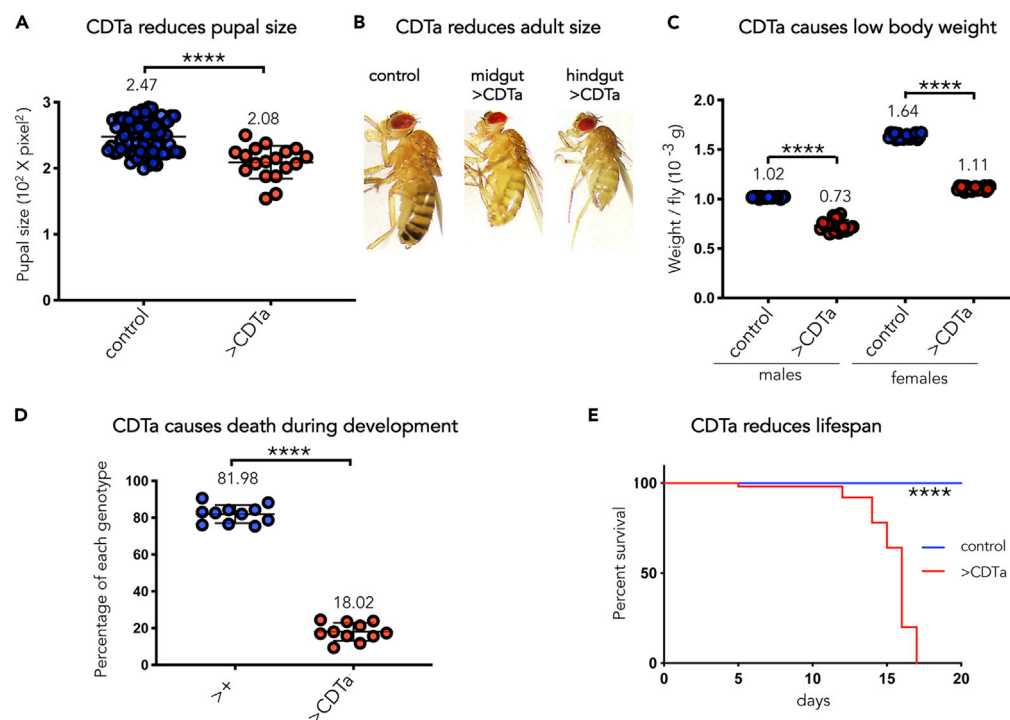


Figure 1. CDTa expression in the Gut Reduces *Drosophila* Pupal and Adult Size, Adult Body Weight, Viability, and Lifespan

(A) Comparative size measurements of NP1GAL4/+ (control) and CDTa-expressing pupae driven by enterocyte-specific NP1GAL4 (>CDTa), grown at room temperature (RT) ($p < 0.0001$). Data are represented as mean \pm SD, here and in subsequent figures.

(B) Images of NP1/+ (control), NP1GAL4>CDTa (midgut > CDTa), and CDTa-expressing adult female flies under the control of a Hindgut-GAL4 driver (hindgut > CDTa) raised at RT. All images were taken at the same magnification.

(C) Comparative body weight measurements of male and female NP1/+ (control) and NP1GAL4>CDTa (>CDTa) flies, raised at RT (males: $p < 0.0001$, females: $p < 0.0001$). Flies were weighed in groups of 10–15. Average weight/fly is plotted for each group.

(D) Comparative rate of emerging adult flies expressing CDTa driven by NP1GAL4 (>CDTa) versus control individuals NP1/+ (>+, flies inheriting the TM6 balancer chromosome instead of the UAS-CDTa transgene) at RT ($p < 0.0001$).

(E) Comparative survival curves between tubGAL80ts NP1/+ (control) and tubGAL80ts NP1>CDTa (>CDTa) male flies at 29°C (the permissive temperature that allows CDTa expression in tubGAL80ts NP1>CDTa flies) (log rank [Mantel-Cox] test = $p < 0.0001$). Three vials of each genotype containing 15 flies each were monitored daily for surviving flies. Surviving flies were transferred to clean vials every 3 days. In (A, C, and D) Data are represented as mean \pm SD. p-values were obtained from unpaired T-tests.

matter, CDTa-expressing flies exhibited markedly reduced defecation (Figure 2A, see lower graph for quantifications). These flies also displayed enlarged and dilated crops (a food storage organ connected to the digestive system in insects) filled with sucrose solution, whereas crops in control flies were smaller and more compact (see green arrows in upper and lower panels of Figure 2B). In addition, CDTa-expressing flies exhibited colored liquid droplets concentrated in their mouthparts, which may reflect compensatory feeding or regurgitation (see black arrows in upper panels). Thus, CDTa expression in the adult fly gut causes retention of feces, possibly resulting from an impairment in intestinal transit.

CDTa Expression Impacts F-actin Network and Tissue Thickness in Wing Imaginal Discs and the Brush Border in Gut Epithelium

Previous studies have demonstrated that CDTa causes F-actin depolymerization in mammalian systems (Aktories, 1994; Aktories and Wegner, 1992; Schwan et al., 2009; Wegner and Aktories, 1988). To assess whether CDTa has a similar activity in fly tissues, we monitored its effects upon expression in wing imaginal discs (Figures 3A–3C), salivary glands (Figure S1), and gut epithelium (Figures 3D and 3E). Ubiquitous CDTa expression in the developing wing disc using the MS1096-GAL4 driver led to the formation of a small blackened appendage in adulthood (Figure 3A, middle panel, compare with a control wing blade in top

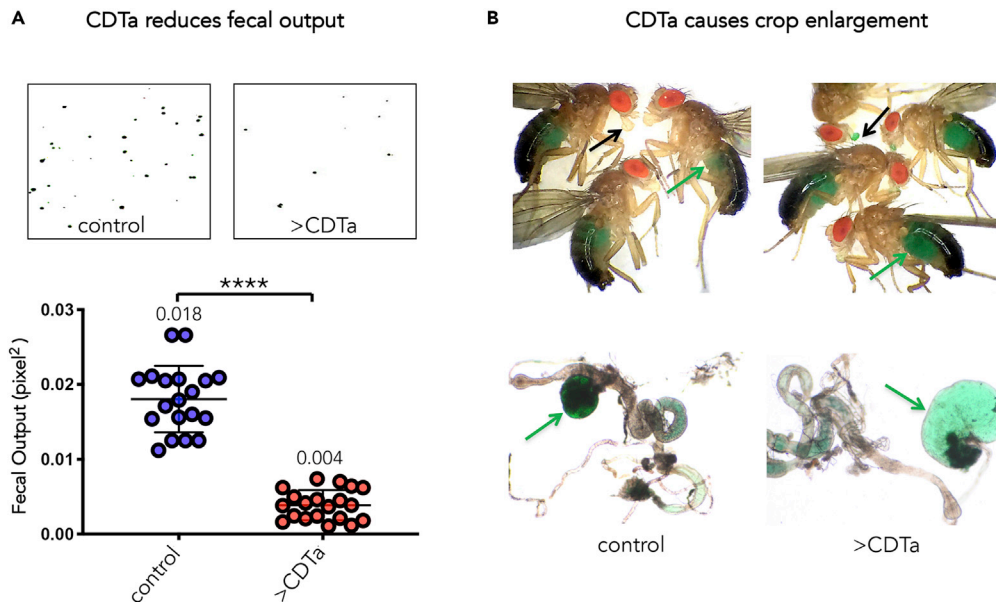


Figure 2. CDTa Expression in the Midgut Reduces Life Span and Fecal Output and Causes Crop Enlargement

(A) Comparative fecal output of 1-week-old tubGAL80ts NP1/+ (control) and CDTa-expressing NP1 tubGAL80ts >CDTa (>CDTa) males, after 1 day exposure to 31°C (to induce CDTa expression in tubGAL80ts NP1>CDTa flies) followed by 3 days of feeding on apple juice-soaked potato flakes supplemented with edible green dye (Mc Cormick, Baltimore, MD) at 31°C. Three vials of each genotype containing 15 flies each were monitored for fecal output deposited on transparent film lining the experimental vials. The film was subsequently scanned and quantified with ImageJ and analyzed using Prism8 ($p < 0.0001$).

(B) Crop size comparison between tubGAL80ts NP1/+ flies (control) and tubGAL80ts NP1>CDTa adult flies (>CDTa) after being fed green apple juice-soaked potato flakes at 31°C for 2–3 days. Photographs of whole flies with abundant green dye visible through the cuticle (upper panels, green arrows) and of dissected guts (lower panels). The green arrows point to the crop, which is enlarged and filled with green fluid in CDTa-expressing animals. Note the proboscis stained with green dye in CDTa-expressing flies, but not in control flies, black arrows.

panel). When CDTa expression was limited to the wing-margin with the VgG4 driver, a notched margin phenotype was observed (Figure 3A, bottom panel). These highly penetrant phenotypes indicate that CDTa interferes with normal wing morphogenesis. We asked whether the observed wing phenotypes derived from a disruption in the actin cytoskeleton during wing development by using fluorescently labeled Phalloidin to stain for F-actin in dissected tissues. Expression of CDTa disrupted the overall integrity of the wing imaginal disc from third-instar larvae, as cells appeared less dense and organized than in control discs (compare top panels in Figure 3B). Overall fluorescence levels were lower in CDTa-expressing discs, indicating a loss in total F-actin. In parallel, wing disc thickness was reduced by 40% compared with controls (lower panels in Figures 3B, see 3C for quantification). Similarly, expression of CDTa in a second larval tissue (salivary glands) greatly reduced F-actin levels, as detected by Phalloidin staining (Figure S1A).

Because *C. difficile* primarily infects the gastrointestinal tract, we focused further analyses on the effect of CDTa expression in the relevant midgut tissue. In wild-type flies, Phalloidin staining of F-actin delineated a well-organized array of cells in both sub-apical and luminal sections of epithelial cells from the anterior midgut (left four panels in Figure 3D). The brush border consisting of F-actin-rich microvilli appeared as a regular polygonal array in sub-apical focal planes and as a thick sinuous line in luminal views. This epithelial actin signal was enclosed by a narrow sheath of bright staining of the muscle layer that surrounds the gut. In contrast, CDTa-expressing guts appeared disorganized with lower F-actin levels and thinner—if any—brush border staining (note that as an internal control, muscle staining was unaltered). Intestinal phenotypes ranged from mildly disorganized epithelial cells (middle four panels in Figure 3D) to barely visible brush borders (right four panels in Figures 3D, see panel 3E for quantification).

In summary, CDTa expression in wing imaginal discs, salivary glands, and midguts severely impacts the F-actin network, reducing total F-actin levels and epithelial thickness and eliminating most of the brush

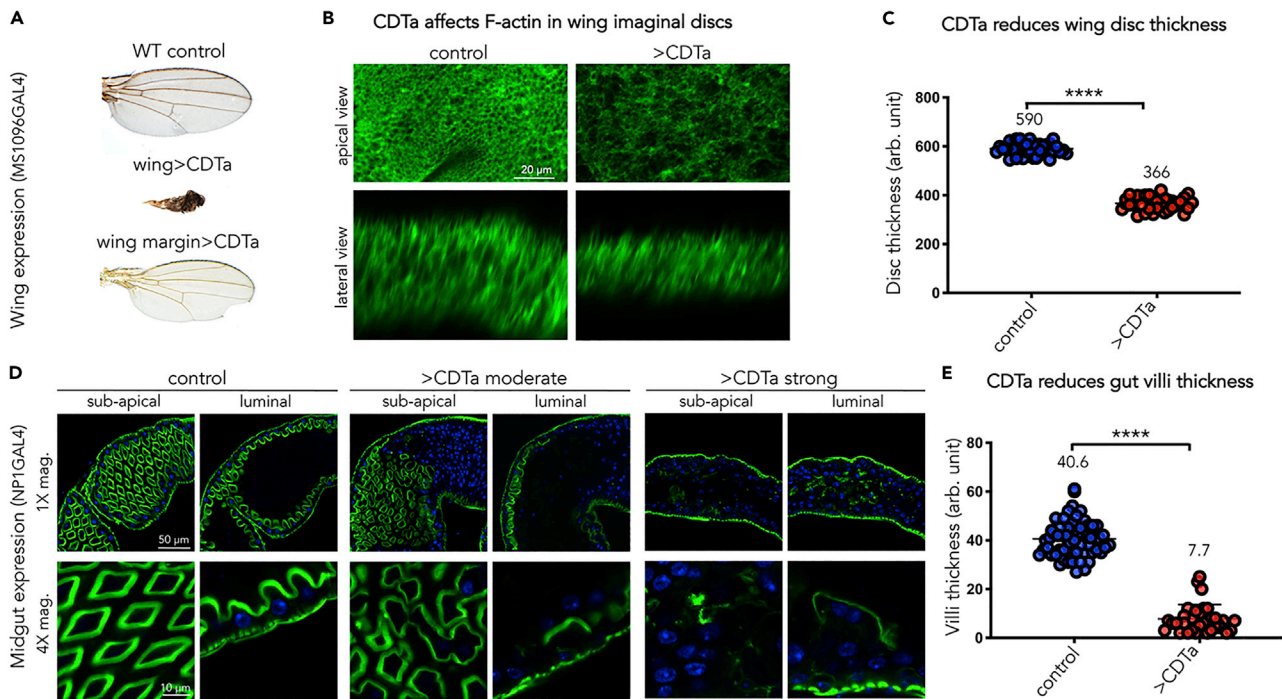


Figure 3. CDTa Disrupts Tissue Integrity and F-actin Network in the Wing and in the Gut Brush Border Epithelium

(A) UAS-CDTa transgenic flies were crossed with individuals from wing-specific GAL4 lines: wing pouch GAL4 MS1096 (wing > CDTa) or wing margin vestigial GAL4 (wing margin > CDTa), and raised at 25°C. All wings (from males) were photographed at the same magnification.

(B) Fluorescent Phalloidin stain of developing wing imaginal discs in wt (control) and wingGAL4>CDTa (>CDTa) male larvae grown at 25°C and imaged by confocal microscopy. Scale bar represents 20 μ m.

(C) Disc thickness was quantified using Photoshop software (Adobe, San Jose, CA), measured in arbitrary units (arb. unit) and analyzed using Prism8 ($p < 0.0001$).

(D) One-week-old tubGAL80ts NP1/+ (control) and CDTa-expressing tubGAL80ts NP1>CDTa male flies (>CDTa) were incubated at 31°C for 24 h. Guts were dissected and stained with Phalloidin-Alexa488 and DAPI (nuclear stain) for confocal microscopy imaging. The anterior section of the midgut, located right before the middle midgut was analyzed in this and subsequent figures. Sub-apical and luminal views taken at 1 \times and 4 \times magnifications (mag.) are shown. Scale bar represents 50 μ m in upper panels and 10 μ m in lower panels.

(E) Intestinal villi thickness was quantified using Photoshop and analyzed using Prism8 ($p < 0.0001$).

See also Figure S1.

border in intestinal cells. The observed loss of microvilli most likely results in the inability to absorb nutrients, which presumably also reduces active bowel transit.

CDTa Alters the Distribution of Rab11 and Key Junctional Proteins

Intercellular junctions are connected to, and depend on, the F-actin network for proper formation and maintenance (Yonemura, 2017). Given the profound disruption of the actin network in cells expressing CDTa, we assessed the effect of this toxin on the distribution and levels of junctional proteins. Adherens junctions are a critical part of the structural framework that maintains tissue integrity, by providing lines of cell-to-cell attachment (Yonemura, 2017). They are composed of trans-membrane Cadherins, which form homodimers with cognate Cadherins expressed by neighboring cells. They also bind to intracellular alpha-Catenins, which serve as a link to actin filaments (Yonemura, 2017; Mège and Ishiyama, 2017). We compared alpha-Catenin distribution in control versus CDTa-expressing guts (Figure 4A). The vast majority of cell junctions in CDTa-expressing enterocytes displayed reduced levels of alpha-Catenin (Figure 4A, thick arrows). Intestinal stem cells, in which the NP1 GAL4 driver is not expressed, retained normal levels of junctional alpha-Catenin, providing an internal control for these experiments (thin arrows in Figure 4A). Rab11, a small GTPase essential for trafficking components to cell junctions, was present throughout the cytoplasm of control intestinal cells and displayed moderate enrichment at the apical plasma membrane (Figure 4B, upper panels). In contrast, Rab11 staining was almost entirely restricted to the apical membrane of CDTa-expressing enterocytes with much lower levels present in the cytoplasm (Figure 4B, lower panels, arrows). These observations are consistent with a previous report that CDTa indirectly deregulates

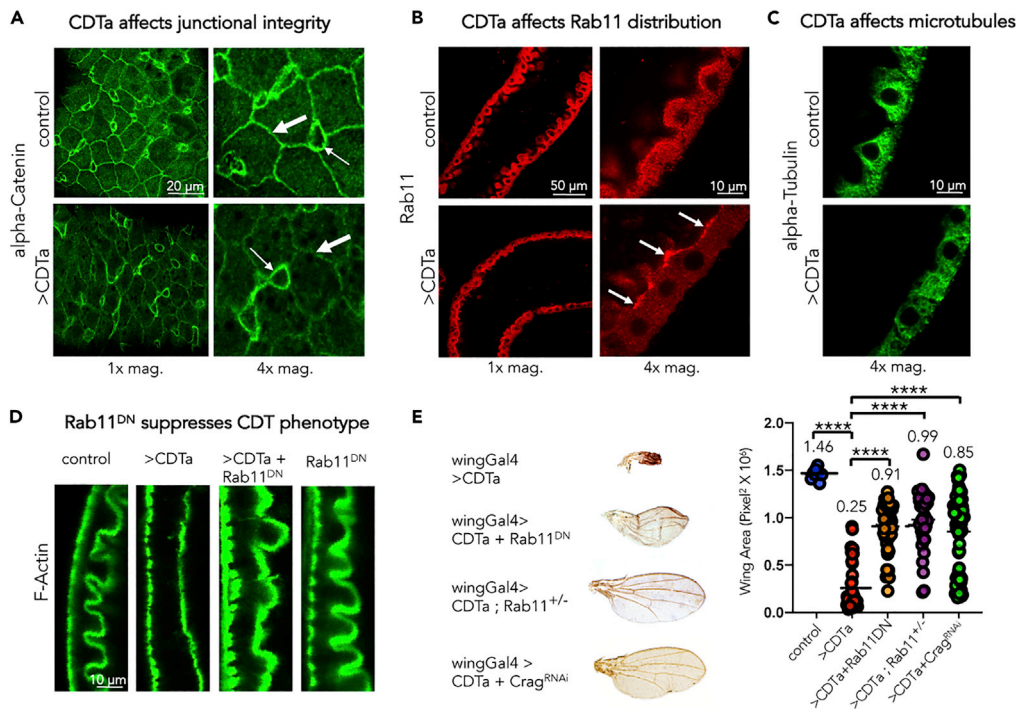


Figure 4. CDTa Affects Junctional Components in the Midgut. Reduction in Rab11 Activity Suppresses CDTa Phenotypes in Gut Brush Border and Wings

(A–C) One-week-old tubGAL80ts NP1/+ (control) and tubGAL80ts NP1>CDTa (>CDTa) male flies were incubated at 31°C for 24 h. Guts were dissected and stained with anti-alpha-Catenin (A), anti-Rab11 (B), or anti-Tubulin antibodies (C). Sub-apical (in A) or luminal views (in B, C, and D) taken at 1× (left panels) or 4× magnifications (A and B, right panels; C and D). In (A), thick arrows point at intercellular junctions stained with the anti-alpha-Catenin antibody. The thin arrows point at intestinal stem cells, in which CDTa is not expressed, showing unchanged levels of alpha-Catenin. Scale bar represents 20 μm. In (B), arrows point at increased apical accumulation of Rab11 in CDTa-expressing enterocytes. Scale bar represents 50 μm in left panels and 10 μm in right panels and for (C).

(D) One-week-old tubGAL80ts NP1/+ (control) +/- Rab11^{DN} and tubGAL80ts NP1>CDTa (>CDTa) +/- Rab11^{DN} male flies were incubated at 31°C for 24 h. Guts were dissected and stained with fluorescent Phalloidin. Scale bar represents 10 μm. (E) Transgenic flies expressing CDTa under the control of wing-specific MS1096 GAL4 (combined with tubGAL80ts) were crossed at 25°C with flies carrying UAS-Rab11^{DN}, Rab11^{J2D/+} (heterozygous recessive loss-of-function mutation, Rab11^{-/+}), UAS-Crag^{RNAi}, or control wt flies. Mounted wings were photographed and surface area was quantified with Photoshop and analyzed using Prism8 (F = 45.85, df = 4, p < 0.0001). Data are represented as mean ± SD. p-values were obtained from one-way ANOVA tests.

See also Figures S2–S5.

Rab11-dependent trafficking (Schwan et al., 2014). This alteration in Rab11 distribution to sites of active transport, which presumably correlates with hyperactivity, contributes to the overall CDTa phenotype since co-expression of CDTa with a dominant negative form of Rab11 (Rab11^{DN}) in the midgut rescued the abnormal brush border caused by CDTa alone (Figure 4D). Similarly, in the developing wing, co-expression of CDTa with Rab11^{DN} suppressed the CDTa phenotype, as did a heterozygous loss-of-function mutation of Rab11 (Figure 4E). We also tested the involvement of Crag (DENND4), the single known Guanine Exchange Factor (GEF) specifically activating Rab11, which was initially discovered as a Calmodulin-binding protein (Xiong et al., 2012). When co-expressed with CDTa, Crag^{RNAi} profoundly rescued the CDTa wing phenotype (Figure 4E). Taken together, these data further support the conserved involvement of Rab11 in accentuating the cellular effect of CDTa.

In CACO-2 cells, CDT induces the formation of microtubule-based membrane protrusions, thus increasing bacterial adherence to host cells (Schwan et al., 2009). To assess whether apical protrusions could be also observed in *Drosophila* intestinal cells, we used these author's protocol to fix CDTa-expressing fly midguts and stained microtubules with an anti-Tubulin antibody (Schwan et al., 2009). Although we were unable to detect any microtubule protrusions extending from CDTa-expressing enterocytes (Figure 4C, lower panel),

or in control tissues (Figure 4C, upper panel), we observed that microtubules in control cells had a clear perinuclear radial distribution (Figure 4C, upper panel), which was less evident in CDTa-expressing enterocytes (Figure 4C, lower panel). A likely consequence of this broad disruption of the cytoskeleton is a loss of epithelial folds observed in CDTa-expressing intestinal tissues (Figures 4B and 4C).

We also examined intercellular junctions in salivary glands, which comprise giant polyploid cells and provide a sensitive system for visualizing junctional components. As described above, CDTa expression in salivary glands caused a severe reduction in F-actin levels (Figure S1A). Mirroring results from intestinal cells, junctional levels of *Drosophila* epithelial Cadherin (DE-cad) were also reduced by CDTa (Figure S1B). Furthermore, Cadherin staining appeared as a spotty signal around lines of cell-cell contact in CDTa-expressing glands, unlike the straight lines of strong contiguous staining typical of control cell junctions (compare panels in Figure S1B). These observations suggest that intercellular junctions were weakened in response to CDTa expression, likely as a direct consequence of F-actin network collapse, which may also be exacerbated by defects in junctional trafficking. Cumulatively, these results reveal that most of the known effects of CDT activity in mammalian cells are recapitulated in *Drosophila* at the molecular, cellular, organ, and organismal levels.

Anthrax Toxin EF Partially Rescues CDTa-Induced Phenotypes

We previously reported that the anthrax toxin Edema Factor (EF), a potent Adenylate Cyclase, inhibits Rab11 activity, leading to junctional defects (Guichard et al., 2017). We therefore wondered whether EF might also block the effects of CDTa. Alone, EF expression causes wing phenotypes consisting of blistered wings with thickened veins and notched margins (Figure S2A, and Guichard et al., 2017; Guichard et al., 2006). Consistent with its inhibitory activity on Rab11, EF partially suppressed the CDTa wing phenotype, leading to an enlarged and partially restored wing blade (Figure S2A, quantified in S2B). Similarly, EF co-expression completely rescued the CDTa-induced salivary gland F-actin phenotype (Figures S2C and S2D) and partially rescued the loss of brush border in the midgut (Figures S2E and S2F). Finally, EF partially rescued other CDTa phenotypes, such as low body weight by 25% (Figure S3A), and improved viability to adulthood by 125% (Figure S3B).

In summary, CDTa-induced phenotypes are rescued by EF expression either partially in wings and midgut tissues, or almost totally in salivary glands, suggesting that EF acts antagonistically to CDTa.

Calmodulin Contributes to CDTa Activity

The calcium (Ca^{2+}) sensor STIM1 (Roos et al., 2005), which resides at the surface of the endoplasmic reticulum (ER), has been shown to play an important role in mediating the activity of CDT in mammalian cells, particularly in the formation of membrane protrusions in CACO-2 cells (Schwan et al., 2014). We tested whether *Drosophila* Stim was also involved in CDTa phenotypes in the wing. We used two RNAi transgenic insertions to reduce Stim expression and co-expressed each of them with CDTa in developing wings. Both Stim RNAi insertions potentially suppressed the CDTa-induced phenotypes, indicating that CDT dependence on the STIM pathway is conserved in *Drosophila* (Figures 5A and 5B).

Since CDT has been shown to trigger Ca^{2+} influx in mammalian cells (Schwan et al., 2014), we also tested whether *Drosophila* Calmodulin (Cam), an ubiquitous cytoplasmic Ca^{2+} sensor, may interact with CDTa activity. As shown in Figure 5A and quantified in Figure 5B, reduction of Cam levels either by expressing a Cam^{RNAi} transgene or by a 50% reduction in Cam gene dosage ($\text{Cam}^{+/-}$), suppressed the CDTa wing phenotype. In contrast, co-expression of CDTa with wild-type Cam (Cam^{WT}) did not alter the effect of the toxin. In control experiments, expression of Cam^{WT} and Cam^{RNAi} alone in the wing did not produce any phenotype, nor did the heterozygous $\text{Cam}^{+/-}$ mutant (Figure S5). Reducing Cam expression by RNAi also rescued the anthrax EF-induced wing phenotype (Figure S4), consistent with EF binding CaM as a required co-factor (Lepple, 1982, 1984). Paralleling observations in the wing, co-expressing Cam^{RNAi} with CDTa in the gut partially rescued the toxin's effect (Figures 5C and 5D), whereas expression of Cam^{RNAi} alone had no discernible effect on the F-actin brush border (Figure 5C). Thus, we conclude that reduction of Cam levels results in suppression of CDTa phenotypes in both gut and wing tissues.

We further explored the involvement of Calmodulin in CDTa activity pharmacologically by using two chemical compounds, Cyclosporin A and FK506, which are known to act as downstream suppressors of Calmodulin via direct interaction with distinct targets, Cyclophilin and FKBP12, respectively (Handschumacher

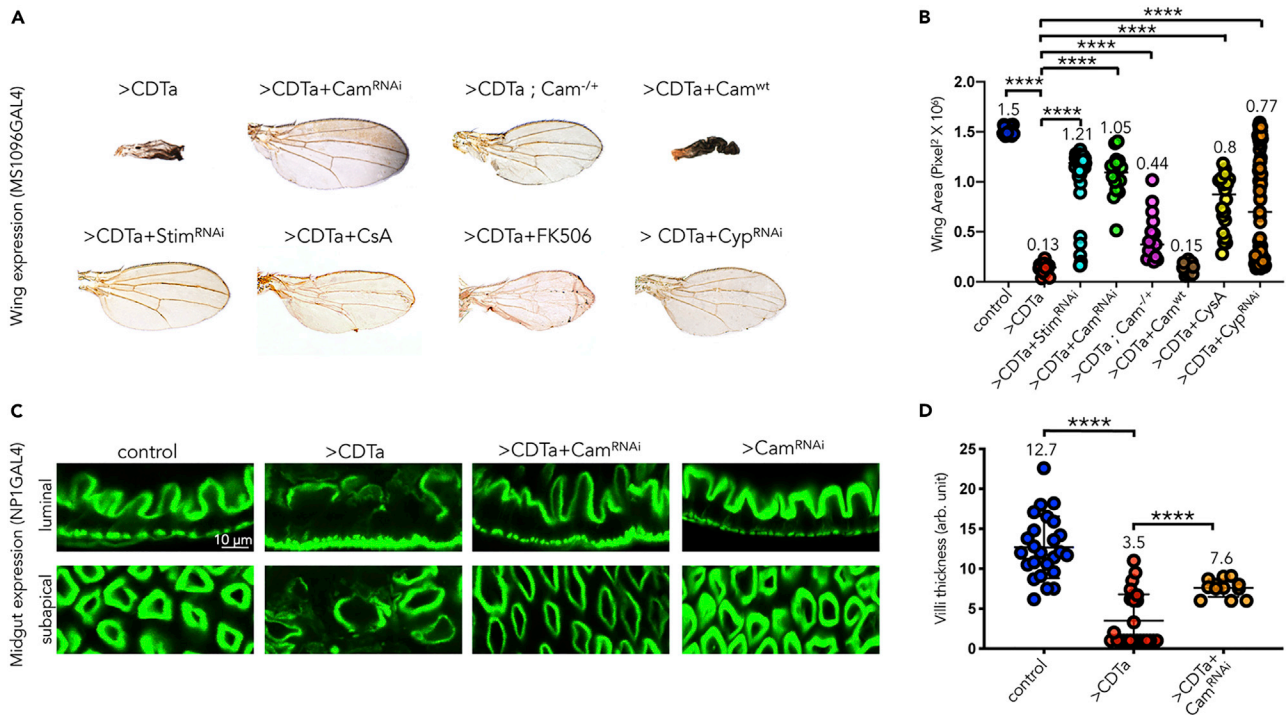


Figure 5. Ca⁺⁺ Signaling Pathway Components Mediate the Downstream Cellular Response to CDTa

(A and B) (A) Wings from adults of indicated genotypes. Male flies expressing CDTa alone under the control of wing-specific MS1096 GAL4 (combined with tubGAL80ts) (>CDTa) or in combination with a UAS-Calmodulin RNAi transgene (>CDTa + Cam^{RNAi}), a heterozygous Cam mutant allele n339 (>CDTa; Cam^{+/-}), a UAS-Stim RNAi transgene (>CDTa + Stim^{RNAi}), a wild-type Cam transgene (>CDTa + Cam^{WT}), a UAS-Cyp RNAi transgene, as well as CDTa-expressing flies treated during development with either Cyclosporin A 40 μ M (Sigma) (>CDTa + CsA) or FK506 50 μ M (Selleckchem.com) (>CDTa + FK506) were grown at 25°C. (B) Surface area from wings shown in (A) were quantified with Photoshop and analyzed using Prism8 (F = 35.55, df = 7, p < 0.0001). See Figure S5 for additional controls.

(C) One-week-old males of the following genotypes: tubGAL80ts NP1/+ (control), tubGAL80ts NP1>CDTa (>CDTa), tubGAL80ts NP1>CDTa + Calmodulin RNAi transgene (>CDTa + Cam^{RNAi}), and tubGAL80ts NP1>Cam^{RNAi} (Cam^{RNAi}) were grown at RT, exposed to 31°C for 1 day, and dissected. Guts were stained with Phalloidin for F-actin and imaged by confocal microscopy. Blocking Calmodulin expression partially rescues CDTa effects on F-actin network. Scale bar represents 10 μ m.

(D) Gut villi thickness was quantified using Photoshop (F = 49.05, df = 2, p < 0.0001). In (B and D) Data are represented as mean \pm SD. p-values were obtained from one-way ANOVA tests.

See Figure S5.

et al., 1984; Liu et al., 1991). As shown in Figures 5A and 5B, CDTa-expressing flies grown in the presence of Cyclosporin A (CsA), FK506, or co-expressing Cyclophilin RNAi, showed clear attenuation of CDTa-induced wing phenotypes. These findings point to the Ca²⁺-induced Cam pathway as an important downstream mediator of CDTa activity, consistent with CDT causing Ca²⁺ influx in intoxicated CACO-2 cells (Schwan et al., 2014). In summary, these results support the hypothesis that CDTa activity is tightly linked to the cellular Ca²⁺ response.

DISCUSSION

Results in this study examine the effects of expressing the *C. difficile* toxin CDTa in *Drosophila*. CDTa-induced phenotypes suggest a strong impairment in digestive functions. For example, CDTa expression in the gut reduces fly body size and weight, compromises viability during development, as well as lowers adult longevity. As expected, considering its mechanism of action in mammalian cells, CDTa significantly reduces F-actin levels in wing imaginal discs, salivary glands, or gut tissues and disrupts F-actin networks and trafficking of key junctional proteins, resulting in a loss of epithelial tissue integrity. In the gut, CDTa expression eliminates most of the actin-rich brush border, which is accompanied by greatly reduced intestinal transit (e.g., crop enlargement and feces retention). Cumulatively, these observations are consistent with CDTa disrupting epithelial integrity and impairing digestive functions.

A significant advantage of *Drosophila* as a model system is the ability to examine genetic interactions with specifically impacted molecular pathways that contribute to the cumulative cellular responses to CDTa. This type of analysis revealed that several effectors were important for mediating the endpoint effects of CDTa, acting downstream of F-actin depolymerization. For example, some of the effects of CDTa require the activity of Rab11, as revealed by suppression of the CDTa wing phenotype either by co-expressing a dominant negative form or a loss-of-function mutation of Rab11, or the anthrax EF toxin, which -like several other virulence factors- has been shown to potently inhibit the Rab11-dependent endocytic recycling pathway (Guichard et al., 2014). Interestingly, previous reports indicate that Rab11 is important for the formation of microvilli, bringing the necessary membrane material surrounding F-actin shafts (Knowles et al., 2015). Thus, the action of CDTa initiated by ADP-ribosylation of actin monomers, impinges on several downstream cellular pathways, which in combination could result in elimination or great reduction of the intestinal brush border. These experiments also revealed that intracellular Ca^{2+} signaling plays an important role in mediating the effects of CDTa. Thus, reducing *Drosophila* Stim or Cam levels suppressed the CDTa wing phenotype, and two drugs acting downstream of Calmodulin (CaM) in the mammalian Ca^{2+} signaling pathway blocked the effect of CDTa during wing development.

In humans, CDIs are the main cause of inflammatory diarrhea after antibiotic treatment, and previous studies in mammalian systems showed that *C. difficile* toxins induce depolymerization of F-actin, leading to deterioration of intestinal microvilli (Abt et al., 2016; Aktories et al., 2018; Just et al., 1995a, 1995b, 1995c; Papatheodorou et al., 2018). Possible complications of CDI are pseudomembranous colitis (PMC), toxic megacolon, perforation of the colon, and sepsis (Martin et al., 2016). PMC is characterized by swelling of the colon with accumulation of inflammatory immune and necrotic cells and formation of Fibrin-rich pseudo-membranes. As summarized above, our results indicate that *Drosophila* recapitulates most known aspects of CDT activity at the molecular, cellular, and tissue levels, with similar loss of F-actin network, loss of epithelial folds, and microvilli deterioration phenotypes. Furthermore, our observation that CDTa causes feces retention and crop enlargement in flies is reminiscent of PMC consistent with suggestions that CDT contributes to intestinal obstruction in patients with CDI (Dingle et al., 2011; Rupnik et al., 2009).

Current knowledge of the molecular mode of action of CDT derives from studies carried out in cultured mammalian cells. In these systems, in addition to actin depolymerization, CDT triggers the formation of protrusions containing microtubules and ER membranes, connected to each other via the calcium sensor STIM1 (Schwan et al., 2014). In addition, CDT causes re-routing of fibronectin-rich vesicles from the basal to the apical side of intestinal epithelial cells in a Rab11-dependent manner, a process guided by Septin polymerization (Nolke et al., 2016), thus enhancing bacterial adherence (Schwan et al., 2014). Although we did not observe any microtubule-rich protrusions in *Drosophila* intestinal cells, our data are consistent with a conservation of the overall cellular response to CDT: in addition to primary disruption of the F-actin network, we observed microtubule redistribution, increased Rab11 localization to the apical side of enterocytes, and weakening of adherens junctions, a likely consequence of both Rab11 dysregulation and F-actin network impairment.

Because CDT elicits Ca^{2+} influx in CACO-2 cells (Schwan et al., 2014), we also evaluated the role of the general Ca^{2+} sensor Cam on the effect of CDTa in our fly system. Reduction in *Drosophila* Cam levels by RNAi or in a *Cam*^{-/+} mutant background rescues the CDTa phenotypes in gut tissues and wings, indicating a previously unappreciated dependence of CDTa activity on the Ca^{2+} /Cam pathway (see model presented in graphical abstract). Blocking expression of another Ca^{2+} sensor, Stim, also counters the effect of CDTa in wings, which is consistent with the known role of mammalian STIM1 in mediating formation of CDT-induced protrusions (Schwan et al., 2014). These latter observations further demonstrate a conservation of the molecular pathways affected by CDT between mammalian systems and flies and validate the use of *Drosophila* as an *in vivo* model for CDTa activity. Interestingly, we found that inhibiting expression of Crag also suppressed CDTa phenotypes in wings. Since Crag is a conserved Calmodulin-binding protein, also acting as a Rab11 GEF (Xiong et al., 2012), it is likely to provide a pivotal link between Cam and Rab11 activities in response to CDTa. Experiments conducted in yeast also revealed that Calcineurin and Ypt3, the yeast homolog of Rab11, are functionally interconnected (Cheng et al., 2002). Although this link has not been mechanistically fully characterized, it may be relevant to the understanding of CDT activity. In our study, two immuno-suppressants known to inhibit Calcineurin, CsA and FK506, which act downstream of CaM, reverted the effect of CDTa in the fly wing, further implicating the *Drosophila* Cam/Calcineurin pathway in the cellular response to CDTa (see model in graphical abstract). Interestingly,

the FK506 compound has also been shown to block cellular entry of several clostridial toxins, including CDT, all of which are ADP-ribosyl transferases (Kaiser et al., 2011, 2012). However, our results cannot be explained by an inhibition of CDTa entry, since we expressed the toxin directly within cells, bypassing the requirement for membrane translocation. Thus, FK506 and CsA block the cellular response downstream of CDTa. Further experiments will be required to assess whether blocking the CaM/Calcineurin pathway with these or related compounds may also have a similar effect in mammalian cells, in addition to their known effects in blocking translocation of CDT across the cell membrane.

Although *C. difficile* is not a known natural fly pathogen, our studies have uncovered striking similarities between the CDT-induced phenotypes in the fly and patho-physiologies associated with CDI in human and mammalian systems. The possibility of studying the effects of *C. difficile* as an infectious pathogen by feeding or injection into flies has not yet been explored. Such studies would be of interest to further characterize the effect of *C. difficile* toxins in an infectious context rather than by simply expressing them in various tissues. Analyzing the effect of CDT in combination with the two other *C. difficile* toxins TcdA and TcdB and assessing whether they act in cooperation to affect Rab11 and Cam would also be interesting to assess potential combinatorial treatments for CDIs.

In conclusion, we describe a transgenic *Drosophila* model that provides a flexible and sensitive system for deciphering the mechanistic pathways that channel the host cellular response to CDT intoxication, operating downstream of G-actin ADP-ribosylation. The ability of inhibitors of the CaM/Calcineurin pathway to block the effect of CDTa in the fly, if replicated in mammalian models, could open the way to potential new therapeutic treatments to alleviate some of the CDI symptoms. Such treatments, however, if proven beneficial, would need to be carefully administered to prevent the toxin's effects while maintaining the necessary immune functions to fight the bacterial infection.

LIMITATIONS OF THE STUDY

Results presented in this report were obtained from experiments performed with transgenic fruit flies expressing the catalytic subunit CDTa in various tissues. Even though *Drosophila* is a well-established genetic model system allowing precise dissection of conserved signaling pathways triggered by CDTa, it is not a mammalian organism. Also, the phenotypes observed are induced by CDTa expression alone, and not part of an infectious process. Therefore, our findings should be validated in mammalian systems such as human cells or mammalian model systems exposed to CDT or infected with *C. difficile*.

METHODS

All methods can be found in the accompanying [Transparent Methods supplemental file](#).

DATA AND CODE AVAILABILITY

Correspondence and request for materials should be addressed to ebier@ucsd.edu or ruschwartz@ucsd.edu

SUPPLEMENTAL INFORMATION

Supplemental Information can be found online at <https://doi.org/10.1016/j.isci.2020.100865>.

ACKNOWLEDGMENTS

We thank Prashant Jain, Jammal Abu-Kazneh, Brian Valadez, and other members of the Bier lab for technical assistance and helpful comments; David Schultz for suggesting testing the CsA and FK506 drugs, and the UCSD School of Medicine Microscopy Core facility (Core Grant P30 NS047101) for microscopy assistance. This work was supported by the National Institutes of Health R01 AI110713 to E.B. and Victor Nizet (UCSD), <https://www.nih.gov/>.

AUTHOR CONTRIBUTIONS

Conceptualization, E.B., A.G., and R.S.; Methodology, R.S.; Validation, R.S., A.G.; Formal Analysis, R.S., A.G.; Investigation, R.S.; Data curation, R.S.; Writing – Original Draft Preparation, N.C.F.; Writing – Review & Editing, R.S., A.G., N.C.F., and E.B.; Visualization, R.S., A.G., N.C.F., S.R.; Supervision, A.G., E.B.; Project Administration, A.G., E.B.; Funding Acquisition, E.B.

DECLARATION OF INTERESTS

E. Bier has equity interest in Synbal Inc. and Agragene, Inc. and also serves on the company's Board of Directors and Scientific Advisory Board. The terms of this arrangement have been reviewed and approved by the University of California, San Diego in accordance with its conflict of interest policies. All other authors declare no competing interests. The funders had no role in study design, data collection and analysis, decision to publish, or preparation of the manuscript.

Received: June 7, 2019

Revised: December 5, 2019

Accepted: January 17, 2020

Published: February 21, 2020

REFERENCES

- Abt, M.C., McKenney, P.T., and Pamer, E.G. (2016). *Clostridium difficile* colitis: pathogenesis and host defence. *Nat. Rev. Microbiol.* **14**, 609–620.
- Aktories, K. (1994). Clostridial ADP-ribosylating toxins: effects on ATP and GTP-binding proteins. *Mol. Cell Biochem.* **138**, 167–176.
- Aktories, K., Barmann, M., Ohishi, I., Tsuyama, S., Jakobs, K.H., and Habermann, E. (1986). Botulinum C2 toxin ADP-ribosylates actin. *Nature* **322**, 390–392.
- Aktories, K., Papatheodorou, P., and Schwan, C. (2018). Binary *Clostridium difficile* toxin (CDT) - a virulence factor disturbing the cytoskeleton. *Anaerobe* **53**, 21–29.
- Aktories, K., Schwan, C., and Jank, T. (2017). *Clostridium difficile* toxin biology. *Annu. Rev. Microbiol.* **71**, 281–307.
- Aktories, K., and Wegner, A. (1992). Mechanisms of the cytopathic action of actin-ADP-ribosylating toxins. *Mol. Microbiol.* **6**, 2905–2908.
- Avet-Rochex, A., Perrin, J., Bergeret, E., and Fauvarque, M.O. (2007). Rac2 is a major actor of *Drosophila* resistance to *Pseudomonas aeruginosa* acting in phagocytic cells. *Genes Cells* **12**, 1193–1204.
- Barth, H., Aktories, K., Popoff, M.R., and Stiles, B.G. (2004). Binary bacterial toxins: biochemistry, biology, and applications of common *Clostridium* and *Bacillus* proteins. *Microbiol. Mol. Biol. Rev.* **68**, 373–402.
- Bartlett, J.G. (2002). Clinical practice. Antibiotic-associated diarrhea. *N. Engl. J. Med.* **346**, 334–339.
- Bartlett, J.G. (2006). Narrative review: the new epidemic of *Clostridium difficile*-associated enteric disease. *Ann. Intern. Med.* **145**, 758–764.
- Bier, E., and Guichard, A. (2012). Deconstructing host-pathogen interactions in *Drosophila*. *Dis. Model. Mech.* **5**, 48–61.
- Blow, N.S., Salomon, R.N., Garrity, K., Reveillaud, I., Kopin, A., Jackson, F.R., and Watnick, P.I. (2005). *Vibrio cholerae* infection of *Drosophila melanogaster* mimics the human disease cholera. *PLoS Pathog.* **1**, e8.
- Botham, C.M., Wandler, A.M., and Guillemin, K. (2008). A transgenic *Drosophila* model demonstrates that the *Helicobacter pylori* CagA protein functions as a eukaryotic Gab adaptor. *PLoS Pathog.* **4**, e1000064.
- Brand, A.H., and Perrimon, N. (1993). Targeted gene expression as a means of altering cell fates and generating dominant phenotypes. *Development* **118**, 401–415.
- Buchon, N., Broderick, N.A., and Lemaître, B. (2013). Gut homeostasis in a microbial world: insights from *Drosophila melanogaster*. *Nat. Rev. Microbiol.* **11**, 615–626.
- Capo, F., Wilson, A., and Di Cara, F. (2019). The intestine of *Drosophila melanogaster*: an emerging versatile model system to study intestinal epithelial homeostasis and host-microbial interactions in humans. *Microorganisms* **7**, <https://doi.org/10.3390/microorganisms7090336>.
- Cheng, H., Sugiura, R., Wu, W., Fujita, M., Lu, Y., Sio, S.O., Kawai, R., Takegawa, K., Shuntoh, H., and Kuno, T. (2002). Role of the Rab GTP-binding protein Ypt3 in the fission yeast exocytic pathway and its connection to calcineurin function. *Mol. Biol. Cell* **13**, 2963–2976.
- Ciaran. (2008). *Clostridium difficile*. *N. Engl. J. Med.* **359**, 1932–1940.
- Dingle, K.E., Griffiths, D., Didelot, X., Evans, J., Vaughan, A., Kachrimanidou, M., Stoesser, N., Jolley, K.A., Golubchik, T., Harding, R.M., et al. (2011). Clinical *Clostridium difficile*: clonality and pathogenicity locus diversity. *PLoS One* **6**, e19993.
- Gerding, D.N., Johnson, S., Rupnik, M., and Aktories, K. (2014). *Clostridium difficile* binary toxin CDT: mechanism, epidemiology, and potential clinical importance. *Gut Microbes* **5**, 15–27.
- Geric, B., Rupnik, M., Gerding, D.N., Grabnar, M., and Johnson, S. (2004). Distribution of *Clostridium difficile* variant toxinotypes and strains with binary toxin genes among clinical isolates in an American hospital. *J. Med. Microbiol.* **53**, 887–894.
- Goncalves, C., Decre, D., Barbut, F., Burghoffer, B., and Petit, J.C. (2004). Prevalence and characterization of a binary toxin (actin-specific ADP-ribosyltransferase) from *Clostridium difficile*. *J. Clin. Microbiol.* **42**, 1933–1939.
- Guichard, A., Cruz-Moreno, B., Aguilar, B., van Sorge, N.M., Kuang, J., Kurkciyan, A.A., Wang, Z., Hang, S., Pineton de Chambrun, G.P., McCole, D.F., et al. (2013). Cholera toxin disrupts barrier function by inhibiting exocyst-mediated trafficking of host proteins to intestinal cell junctions. *Cell Host Microbe* **14**, 294–305.
- Guichard, A., Jain, P., Moayeri, M., Schwartz, R., Chin, S., Zhu, L., Cruz-Moreno, B., Liu, J.Z., Aguilar, B., Hollands, A., et al. (2017). Anthrax edema toxin disrupts distinct steps in Rab11-dependent junctional transport. *PLoS Pathog.* **13**, e1006603.
- Guichard, A., McGillivray, S.M., Cruz-Moreno, B., van Sorge, N.M., Nizet, V., and Bier, E. (2010). Anthrax toxins cooperatively inhibit endocytic recycling by the Rab11/Sec15 exocyst. *Nature* **467**, 854–858.
- Guichard, A., Nizet, V., and Bier, E. (2014). RAB11-mediated trafficking in host-pathogen interactions. *Nat. Rev. Microbiol.* **12**, 624–634.
- Guichard, A., Park, J.M., Cruz-Moreno, B., Karin, M., and Bier, E. (2006). Anthrax lethal factor and edema factor act on conserved targets in *Drosophila*. *Proc. Natl. Acad. Sci. U S A* **103**, 3244–3249.
- Handschumacher, R.E., Harding, M.W., Rice, J., Drugge, R.J., and Speicher, D.W. (1984). Cyclophilin: a specific cytosolic binding protein for cyclosporin A. *Science* **226**, 544–547.
- Just, I., and Gerhard, R. (2004). Large clostridial cytotoxins. *Rev. Physiol. Biochem. Pharmacol.* **152**, 23–47.
- Just, I., Selzer, J., von Eichel-Streiber, C., and Aktories, K. (1995a). The low molecular mass GTP-binding protein Rho is affected by toxin A from *Clostridium difficile*. *J. Clin. Invest.* **95**, 1026–1031.
- Just, I., Selzer, J., Wilm, M., von Eichel-Streiber, C., Mann, M., and Aktories, K. (1995b). Glucosylation of Rho proteins by *Clostridium difficile* toxin B. *Nature* **375**, 500–503.
- Just, I., Wilm, M., Selzer, J., Rex, G., von Eichel-Streiber, C., Mann, M., and Aktories, K. (1995c). The enterotoxin from *Clostridium difficile* (ToxA) monoglucosylates the Rho proteins. *J. Biol. Chem.* **270**, 13932–13936.
- Kaiser, E., Böhm, N., Ernst, K., Langer, S., Schwan, C., Aktories, K., Popoff, M., Fischer, G., and Barth, H. (2012). FK506-binding protein 51 interacts with

Clostridium botulinum C2 toxin and FK506 inhibits membrane translocation of the toxin in mammalian cells. *Cell Microbiol.* 14, 1193–1205.

Kaiser, E., Kroll, C., Ernst, K., Schwan, C., Popoff, M., Fischer, G., Buchner, J., Aktories, K., and Barth, H. (2011). Membrane translocation of binary actin-ADP-ribosylating toxins from *Clostridium difficile* and *Clostridium perfringens* is facilitated by cyclophilin A and Hsp90. *Infect. Immun.* 79, 3913–3921.

Kelly, C.P., and LaMont, J.T. (2008). *Clostridium difficile*—more difficult than ever. *N. Engl. J. Med.* 359, 1932–1940.

Knowles, B.C., Weis, V.G., Yu, S., Roland, J.T., Williams, J.A., Alvarado, G.S., Lapierre, L.A., Shub, M.D., Gao, N., and Goldenring, J.R. (2015). Rab11a regulates syntaxin 3 localization and microvillus assembly in enterocytes. *J. Cell Sci.* 128, 1617–1626.

Leppla, S.H. (1982). Anthrax toxin edema factor: a bacterial adenylate cyclase that increases cyclic AMP concentrations of eukaryotic cells. *Proc. Natl. Acad. Sci. U S A* 79, 3162–3166.

Leppla, S.H. (1984). Bacillus anthracis calmodulin-dependent adenylate cyclase: chemical and enzymatic properties and interactions with eucaryotic cells. *Adv. Cyclic Nucleotide Protein Phosphorylation Res.* 17, 189–198.

Lessa, F.C., Mu, Y., Bamberg, W.M., Beldavs, Z.G., Dumyati, G.K., Dunn, J.R., Farley, M.M., Holzbauer, S.M., Meek, J.I., Phipps, E.C., et al. (2015). Burden of *Clostridium difficile* infection in the United States. *N. Engl. J. Med.* 372, 825–834.

Liu, J., Farmer, J.D., Jr., Lane, W.S., Friedman, J., Weissman, I., and Schreiber, S.L. (1991). Calcineurin is a common target of cyclophilin-cyclosporin A and FKBP-FK506 complexes. *Cell* 66, 807–815.

Luo, L., Matthews, J.D., Robinson, B.S., and Jones, R.M. (2019). *Vibrio parahaemolyticus* VopA is a potent inhibitor of cell migration and apoptosis in the intestinal epithelium of *Drosophila melanogaster*. *Infect. Immun.* 87, e00669–e00618.

Martin, J.S., Monaghan, T.M., and Wilcox, M.H. (2016). *Clostridium difficile* infection:

epidemiology, diagnosis and understanding transmission. *Nat. Rev. Gastroenterol. Hepatol.* 13, 206–216.

McGuire, S.E., Mao, Z., and Davis, R.L. (2004). Spatiotemporal gene expression targeting with the TARGET and gene-switch systems in *Drosophila*. *Sci. STKE* 2004, pl6.

Mège, R.M., and Ishiyama, N. (2017). Integration of cadherin adhesion and cytoskeleton at *adherens* junctions. *Cold Spring Harb. Perspect. Biol.* 9, a028738.

Nolke, T., Schwan, C., Lehmann, F., Ostevold, K., Pertz, O., and Aktories, K. (2016). Septins guide microtubule protrusions induced by actin-depolymerizing toxins like *Clostridium difficile* transferase (CDT). *Proc. Natl. Acad. Sci. U S A* 113, 7870–7875.

Papatheodorou, P., Barth, H., Minton, N., and Aktories, K. (2018). Cellular uptake and mode-of-action of *Clostridium difficile* toxins. *Adv. Exp. Med. Biol.* 1050, 77–96.

Papatheodorou, P., Carette, J.E., Bell, G.W., Schwan, C., Guttenberg, G., Brummelkamp, T.R., and Aktories, K. (2011). Lipolysis-stimulated lipoprotein receptor (LSR) is the host receptor for the binary toxin *Clostridium difficile* transferase (CDT). *Proc. Natl. Acad. Sci. U S A* 108, 16422–16427.

Popoff, M.R., Rubin, E.J., Gill, D.M., and Boquet, P. (1988). Actin-specific ADP-ribosyltransferase produced by a *Clostridium difficile* strain. *Infect. Immun.* 56, 2299–2306.

Roos, J., DiGregorio, P.J., Yeromin, A.V., Ohlsen, K., Lioudyno, M., Zhang, S., Safrina, O., Kozak, J.A., Wagner, S.L., Cahalan, M.D., et al. (2005). STIM1, an essential and conserved component of store-operated Ca²⁺ channel function. *J. Cell Biol.* 169, 435–445.

Rupnik, M., Wilcox, M.H., and Gerding, D.N. (2009). *Clostridium difficile* infection: new developments in epidemiology and pathogenesis. *Nat. Rev. Microbiol.* 7, 526–536.

Schindelin, J., Arganda-Carreras, I., Frise, E., Kaynig, V., Longair, M., Pietzsch, T., Preibisch, S., Rueden, C., Saalfeld, S., Schmid, B., et al. (2012).

Fiji: an open-source platform for biological-image analysis. *Nat. Methods* 9, 676–682.

Schwan, C., Krupke, A.S., Nolke, T., Schumacher, L., Koch-Nolte, F., Kudryashev, M., Stahlberg, H., and Aktories, K. (2014). *Clostridium difficile* toxin CDT hijacks microtubule organization and reroutes vesicle traffic to increase pathogen adherence. *Proc. Natl. Acad. Sci. U S A* 111, 2313–2318.

Schwan, C., Stecher, B., Tzivelekidis, T., van Ham, M., Rohde, M., Hardt, W.D., Wehland, J., and Aktories, K. (2009). *Clostridium difficile* toxin CDT induces formation of microtubule-based protrusions and increases adherence of bacteria. *PLoS Pathog.* 5, e1000626.

Stiles, B.G., Pradhan, K., Fleming, J.M., Samy, R.P., Barth, H., and Popoff, M.R. (2014). *Clostridium* and *Bacillus* binary enterotoxins: bad for the bowels, and eukaryotic being. *Toxins (Basel)* 6, 2626–2656.

Stubbs, S., Rupnik, M., Gibert, M., Brazier, J., Duerden, B., and Popoff, M. (2000). Production of actin-specific ADP-ribosyltransferase (binary toxin) by strains of *Clostridium difficile*. *FEMS Microbiol. Lett.* 186, 307–312.

Vandekerckhove, J., Schering, B., Barmann, M., and Aktories, K. (1987). *Clostridium perfringens* iota toxin ADP-ribosylates skeletal muscle actin in Arg-177. *FEBS Lett.* 225, 48–52.

Voth, D.E., and Ballard, J.D. (2005). *Clostridium difficile* toxins: mechanism of action and role in disease. *Clin. Microbiol. Rev.* 18, 247–263.

Wegner, A., and Aktories, K. (1988). ADP-ribosylated actin caps the barbed ends of actin filaments. *J. Biol. Chem.* 263, 13739–13742.

Xiong, B., Bayat, V., Jaiswal, M., Zhang, K., Sandoval, H., Charng, W.L., Li, T., David, G., Duraine, L., Lin, Y.Q., et al. (2012). Crag is a GEF for Rab11 required for rhodopsin trafficking and maintenance of adult photoreceptor cells. *PLoS Biol.* 10, e1001438.

Yonemura, S. (2017). Actin filament association at *adherens* junctions. *J. Med. Invest.* 64, 14–19.

iScience, Volume 23

Supplemental Information

A Drosophila Model

for *Clostridium difficile* Toxin CDT Reveals

Interactions with Multiple Effector Pathways

Ruth Schwartz, Annabel Guichard, Nathalie C. Franc, Sitara Roy, and Ethan Bier

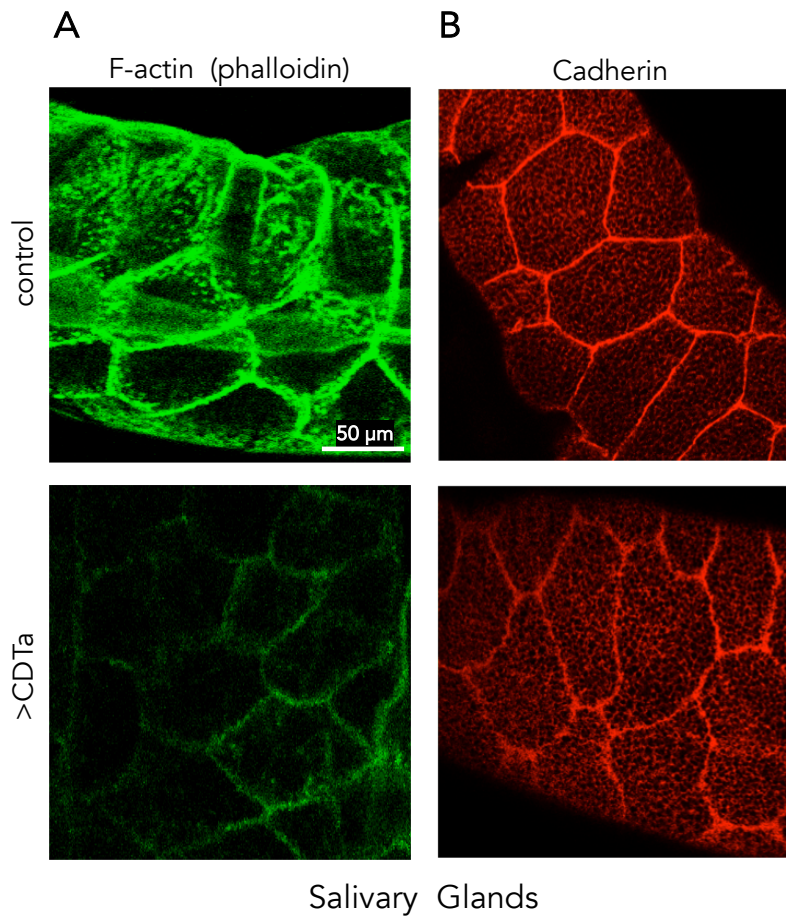


Figure S1. CDTa expression disrupts F-actin network and tissue morphology in salivary glands, related to Fig 3.

Salivary glands from wt (control) or CDTa-expressing third instar larvae under the control of the MS1096-GAL4 (>CDTa) were dissected and stained with fluorescent Phalloidin, which binds actin filaments (F-actin) (left panels) or with an anti-Cadherin antibody, which stains adherens junctions (right panels). Scale bar represents 50 μm.

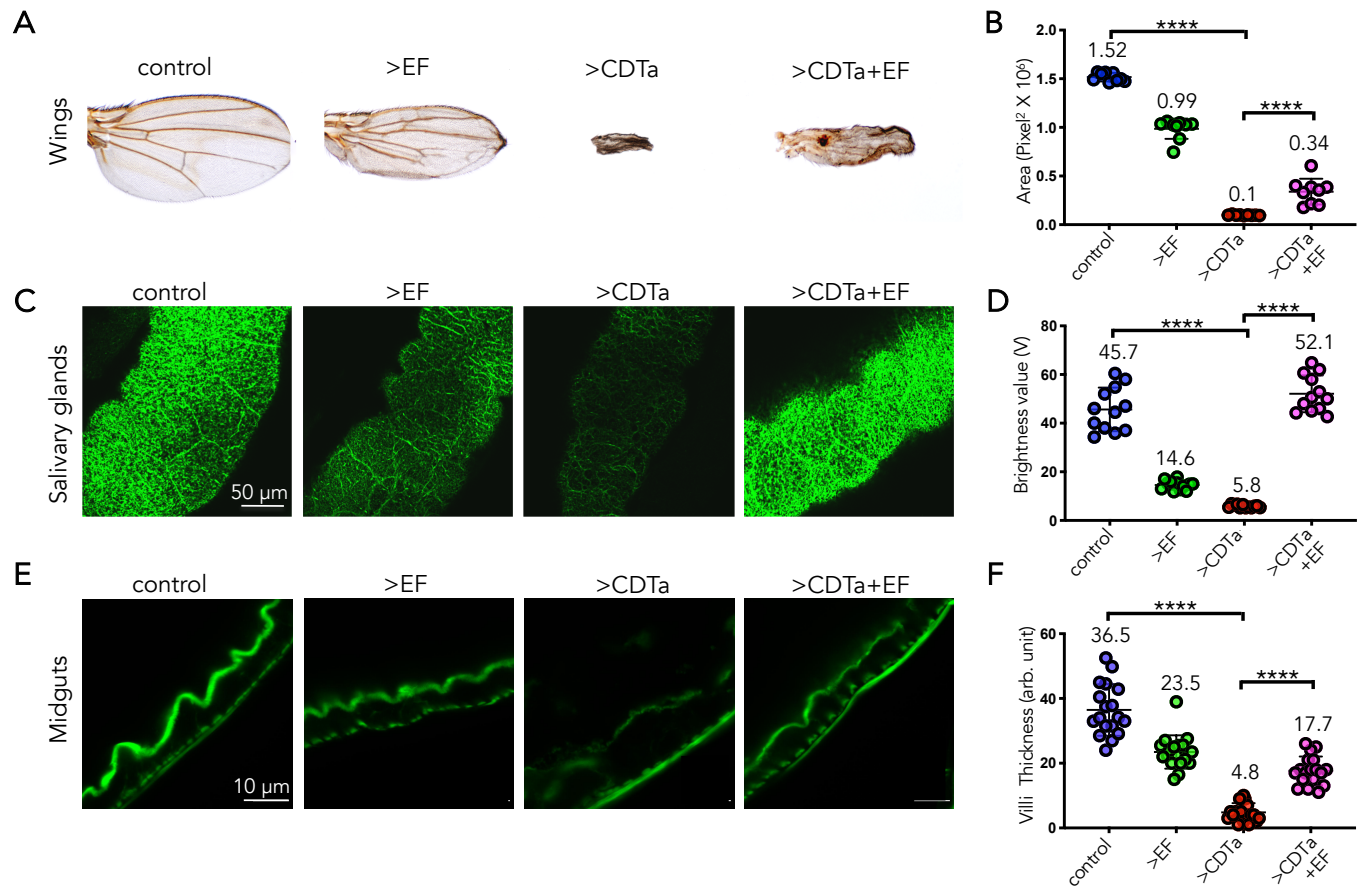
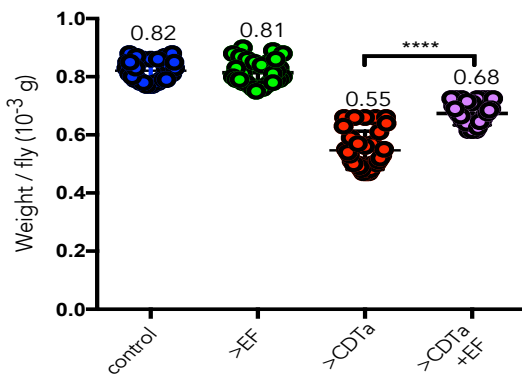


Figure S2. Anthrax EF toxin partially rescues CDTa phenotypes in wings, salivary glands and guts. Related to Fig 4.

(A) Wings from male flies of indicated genotypes grown at 25°C. Male flies expressing CDTa under the control of wing-specific tubGAL80ts MS1096 (>CDTa), tubGAL80ts MS1096 EF (>EF) or in combination (>CDTa+EF) are shown. Co-expression of anthrax EF toxin partially rescues the strong CDTa wing phenotype. (B) Mounted wings shown in A were photographed and surface area was quantified with Photoshop® (F=490.6, df=3, p<0.0001). (C) Salivary glands from third instar larvae grown at 25°C and stained with fluorescent Phalloidin. Genotypes are the same as in panel A. EF expression fully

rescues the loss of F-actin seen in CDTa-expressing glands. (D) Fluorescence levels were measured with ImageJ ($F=175.3$, $df=3$, $p<0.0001$). (E) One week-old adult control males, or expressing EF, CDTa or both under tubGAL80ts NP1 were grown at RT, further incubated for 24hrs at 31°C and dissected. F-actin in gut cells was stained with fluorescent Phalloidin. EF partially rescues villi thickness when co-expressed with CDTa. Midgut images are luminal views. Scale bar represents 50 μm in upper panels and 10 μm in lower panels. (F) Comparative measurements of villi thickness were quantified with Photoshop® and analyzed using Prism8 ($F=105.5$, $df=3$, $p<0.0001$).

A EF partially rescues CDTa-induced low body weight



B EF partially rescues CDTa-induced pre-adult lethality

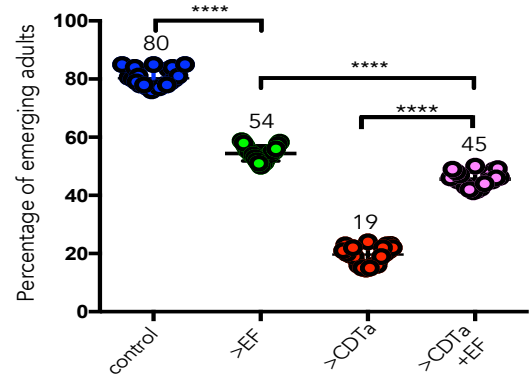


Figure S3. Anthrax EF toxin expression rescues both CDTa-induced body weight and viability to adulthood phenotypes, related to Fig 4.

(A) Comparative body weight of flies of the following genotypes: tubGAL80ts NP1/+ (control), tubGAL80ts NP1>EF (>EF), tubGAL80ts NP1>CDTa (>CDTa), and tubGAL80ts NP1>CDTa and EF (>CDTa+EF). Animals were raised at 25°C. Data was analyzed using Prism8 (F=249.6, df=3, p<0.0001). (B) Comparative survival to adulthood at 25°C. Same genotypes as in panel A are indicated. Data was analyzed using Prism8 (F=1176, df=3, p<0.0001).

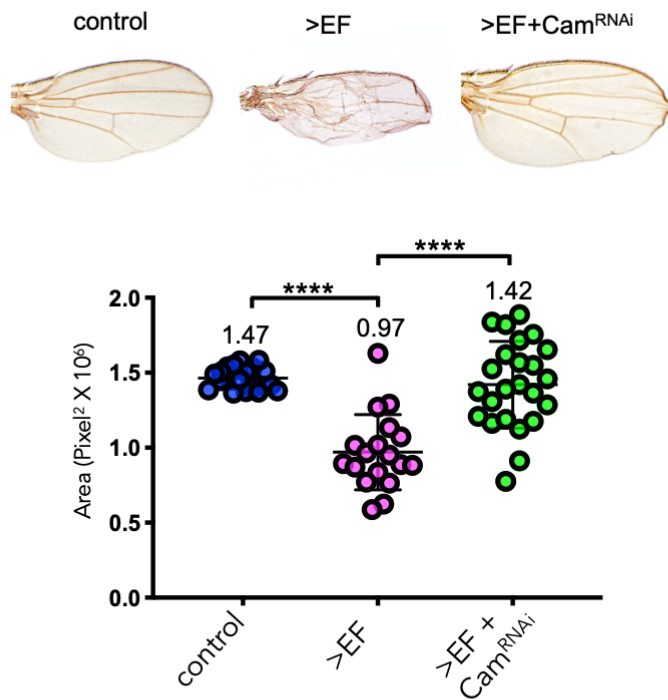


Figure S4. EF activity depends on Calmodulin, related to Figure 4.

Wings from female flies of the following genotypes: wt (control), MS1096 GAL4 tubGAL80ts > EF (>EF), MS1096 GAL4 tubGAL80ts > EF + Cam^{RNAi}, (>EF+Cam^{RNAi}). Flies were grown at 25°C. Their respective wing phenotypes were photographed, and the surface area of the wings quantified with Photoshop® and analyzed using Prism8 (F=27.12, df=2, p<0.0001).

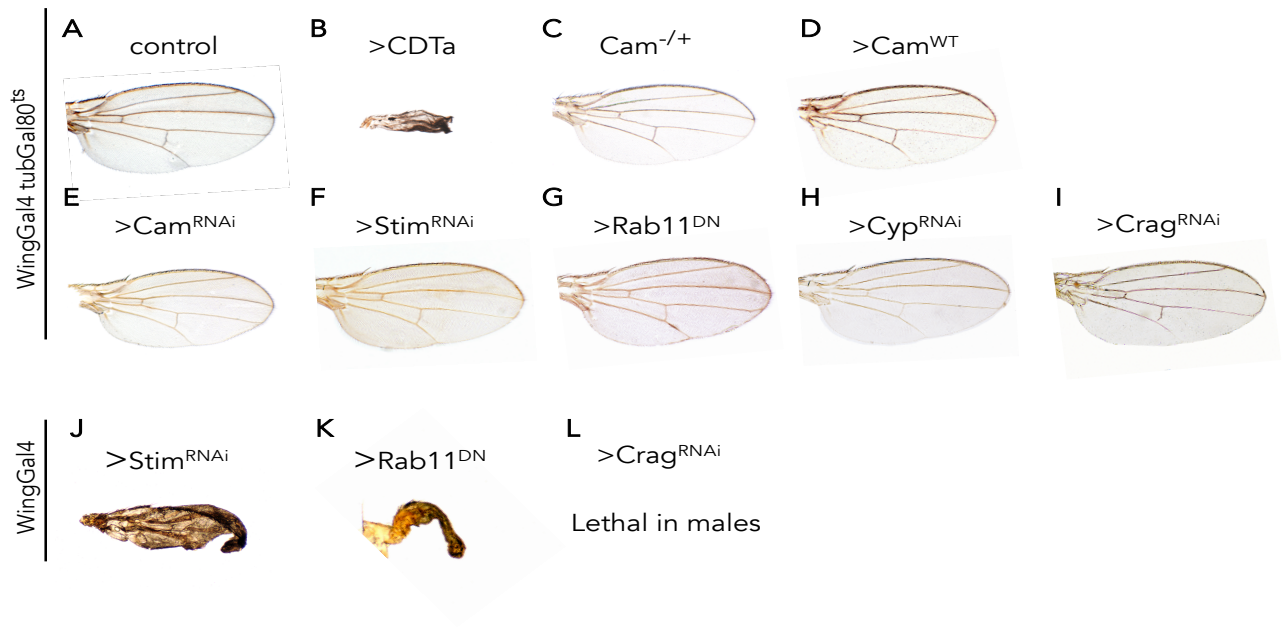


Figure S5. Wing phenotypes from flies expressing various transgenes. Related to figures 4 and 5.

Phenotypes of wings obtained from male flies grown at with 25°C, specific genotypes are indicated. In the two upper rows, tubGAL80ts partially inhibits GAL4-dependent expression of the indicated transgenes. Except for UAS-CDTa, all transgenes in this study do not induce a phenotype when driven by MS1096 GAL4 + tubGAL80ts. On the third row, wing phenotypes in absence of tubGAL80ts, when applicable, are shown: Stim^{RNAi} and Rab11^{DN} induce clear wing phenotypes or lethality (Crag^{RNAi}) when driven by MS1096 GAL4 without tubGAL80ts suppression. All other transgenes did not induce any wing phenotype, even in the absence of tubGAL80-ts.

TRANSPARENT METHODS

Ethics statement.

All experiments were performed in strict accordance with guidelines from the National Institute of Health and the Animal Welfare Act, approved by the Animal Care and Use Committee of University of California, San Diego and the National Institute of Allergy and Infectious Diseases, National Institutes of Health (approved protocols s00227m and LPD-8E). All efforts were made to minimize suffering of animals employed in this study.

UAS-CDTa plasmid construction.

A PCR amplified cDNA fragment from *C. difficile* chromosomal DNA (strain R20291) encoding the enzymatically active CDTa moiety was inserted into the pUAS vector between the EcoR1 and Xba1 sites of the polylinker (details available upon request). The UAS-CDTa transgene was stably transformed into the *Drosophila* genome by BestGene. Two lines carrying an insertion on the second or the third chromosome were isolated.

***Drosophila* genetics.**

Flies carrying the UAS-CDTa construct (CDTa) were crossed to various GAL4 driver stocks to drive toxin expression in specific tissues. In some experiments, timing of GAL4 activity was limited by a temperature sensitive form of GAL80 (*tubulin-GAL80ts*), which

inhibits GAL4 function below 25°C. UAS-EF was described previously (Guichard et al., 2010). Other lines used in this study: wingGal4 (MS1096-GAL4), NP1-GAL4, Hindgut-GAL4, VgGal4. Lines obtained from Bloomington *Drosophila* Stock Center (BDSC, Bloomington, IN): UAS-Cam^{RNAi} (P{TRiP.HMS01318}, # 34609), Camⁿ³³⁹/CyO and UAS-Cam^{WT} (both derived from #6809), UAS-Stim^{RNAiE} (#41759), UAS-Stim^{RNAi}JF02567 (#27263), UAS-Crag^{RNAi} (#53261), UAS-Cyp1^{RNAi} (#33950), Rab11^{J2D1}/TM3 (#12148) and UAS-Rab11^{DNYFP} (#23261).

Survival assays.

In survival assays, expression of GAL4 activity was held by a temperature sensitive form of GAL80, which inhibits GAL4 function below 25°C. TubGAL80ts NP1/+ (control) and tubGAL80ts NP1>CDTa (>CDTa) males were grown at RT and transferred to 29°C a week after hatching. Fly survival was monitored daily. Surviving flies were transferred to clean vials dusted with ground potato flakes every three days.

Immunological stains of wing imaginal discs, salivary glands and guts.

Wing imaginal discs and salivary glands were dissected, fixed in 1X PBS with 4% formaldehyde for 30 minutes, stained with either fluorescent Phalloidin or primary antibodies at 4°C overnight; when using primary antibodies, fluorescent secondary antibodies were incubated at RT for two hours. Tissues were left attached to carcasses until ready to mount in SlowFade (LifeTechnologies, Carlsbad, CA, #S36936) as previously described (Guichard et al.). Double sided tape was used as a spacer to prevent tissue squashing.

Guts were dissected, fixed in 1X PBS with 4% formaldehyde for 40 minutes, stained with fluorescent Phalloidin or primary antibodies overnight; when using primary antibodies, fluorescent secondary antibodies were incubated at RT for two hours. Guts were mounted in SlowFade using double sided tape as spacer. The anterior section of the midgut, located right before the middle midgut was selected for imaging. Images were collected by confocal microscopy on a Leica TCS SP5 (Leica, Wetzlar, Germany). Images were acquired using a 63X objective, and higher magnifications were obtained using a 4X digital zoom. Antibodies and dilutions used were as follows: mouse Rab11 (1/200, BD Biosciences, San Jose, CA, #610657, RRID #AB_397984), DE-cad (1/500, DSHB, Iowa city, IA, #DCAD2, RRID #AB_2314298), D-Cat (1/500, DSHB # Dcat-1-s, RRID #AB_532377), mouse anti-Tubulin (1/100, Santa Cruz Biotechnology, Dallas, TX, sc-23948, RRID #AB_628410), Alexa Fluor 488 Phalloidin (1/100, Invitrogen, Carlsbad, CA, A12379, RRID # AB_231514), DAPI (Molecular Probes, Eugene, OR, D-1306, RRID #AB_2619482).

Data Presentation and Statistics.

Numerical data is presented as mean +/-SD. All graphs were generated and statistics calculated using the Prism-GraphPad software (San Diego, CA). T-test statistical analyses were performed whenever two conditions were compared to each other. When more than two conditions are presented in one graph, we performed ANOVA analysis. For survival assays we performed a log-rank (Mantel–Cox) test. All p values are provided in the figures. **** Indicates $p < 0.0001$.

Wing phenotype analysis.

Measurements of the surface area of multiple wings for each genotype and condition were conducted using Photoshop® and analyzed with Prism8.